Electronic supplementary information

X‑ray Spectroscopy Uncovering the Effects of Cu Based Nanoparticle Concentration and Structure on *Phaseolus vulgaris* Germination and Seedling Development

Nádia M. Duran[a], Susilaine M. Savassa[a], Rafael Giovanini de Lima[a], Eduardo de Almeida[a], Francisco S. Linhares[b,] Cornelis A. M. van Gestel[c], and Hudson W. Pereira de Carvalho[a,]*

[a]Laboratory of Nuclear Instrumentation (LIN), Center of Nuclear Energy in Agriculture (CENA), University of São Paulo (USP), Piracicaba, SP, 13416000, Brazil.

[b]Laboratory of Plant Development and Structure (LaBDEV), Center of Nuclear Energy in Agriculture (CENA), University of São Paulo (USP), Piracicaba, SP, 13416-000, Brazil.

[c]Department of Ecological Science, Faculty of Sciences, Vrije Universiteit, De Boelelaan 1085, 1081HV Amsterdam, The Netherlands.

*Corresponding author:

E-mail: hudson@cena.usp.br

Phone: + 55 19 3429 4737

Contents

Table S1 presents a bibliographic survey regarding the effects of Ag, ZnO, Fe, and CuO nanoparticles treatment on seeds.

Table S1. Bibliographic survey of nanoparticle seed treatment. Symbols used in the table: ↑= Increase, ↓= Decrease.

Ref.	Species	Conc. (mg L^{-1})	Type	Size (nm)	Time of exposure	Main visual effects
1	*Pennisetum glaucum* (pearl millet)	20 and 50	Ag	13	2 h	↑ germination rate and ↓ seedlings growth
2	*Oryza sativa* L. cv. *KDML 105* (jasmine rice)	0.1, 1, 10, 100 and 1,000	Ag	20, 30–60, 70–120 and 150	24 h	↓ germination rate and seedlings growth
3	*Zea mays L.* (corn)	10, 100 and 1,000	ZnO	30 ± 12	2 h	↑ root elongation at 10 mg L^{-1} and ↓ at 1,000 mg L^{-1}
3	*Cucumis sativus L.* (cucumber)	10, 100 and 1,000	ZnO	30 ± 12	2 h	↓ root elongation
4	*Abelmoschus esculentus* (L.) Moench (okra)	50 100, 200 and 500	Zn	<50	24 h	↑ germination rate, ↓ shoot length and ↑ root hairs (except at 500 mg L^{-1})
5	*Pisum sativum L.* (green pea)	50, 100, 200, 400 and 500	CuO	30	14 days	↓ seedling growth (except for 50 mg L^{-1})
6	*Arachis hypogaea* (peanut)	0.56, 1.12, 2.24, 4.48, 8.96 and 17.92	Fe^0	20 – 80	5 days	↑ seedling growth
7	*Brassica pekinensis L.* (chinese cabbage)	1, 5,10, 20, 40 and 80	ZnO	30, 50, 90 and 150	3 days	↓ seedling growth
8	*Vigna radiata L.* (mung bean)	5, 10 20 and 50	Ag	20	21 days	↓ shoot length at 50 mg L^{-1} and ↓ root length at 20 and 50 mg L^{-1}
9	*Triticum aestivum L.* (wheat)	1 and 10	Ag	10	4 h	↓ seedling growth at 10 mg L^{-1}

Contents from the experimental section of the main manuscript

nCuO Characterization

Purity and contaminant analysis of each bulk nano CuO (nCuO) was done by energy dispersive X-ray fluorescence spectroscopy (EDXRF; EDX-720 Shimadzu, Japan). Two hundred milligrams of pristine powders were weighted in a 6.3 mm aperture X-ray fluorescence spectroscopy (XRF) sample cup (no. 3577 - Spex Ind. Inc., USA) sealed with a 5 μm thick polypropylene film (no. 3520 - Spex Ind. Inc., USA). The samples were analyzed under vacuum, in triplicate, using a rhodium (Rh) X-ray tube at 50 kV and auto-tunable current adjusted for a detector deadtime below 30% and a 3-mm collimator. The X-ray spectrum of the sample was acquired utilizing a Si (Li) detector for 300 s.

The crystal structure of the nCuO was determined by X-ray diffraction (XRD) employing a PW 1877 diffractometer (Philips, Netherlands) with Cu-Kα radiation. Using the broadening peak it was possible to estimate the crystallite size by the Scherrer equation:

$$D_{(hkl)} = K\lambda / \boldsymbol{\beta}\cos\theta$$

where D is the mean crystal size of the nanoparticles, K the Scherrer constant (0.94 for spherical crystals with cubic symmetry), λ the wavelength of light used for the diffraction (0.154184 nm to Cu), $\boldsymbol{\beta}$ the full width at half maximum of the peak, and θ refers to the angle measured.

Copper uptake quantification

The Cu content of the digested samples was determined by EDXRF. For Cu determination, 15 μL of the digests were pipetted into the external side window of the 6.3 mm aperture XRF sample cup (no. 3577 - Spex Ind. Inc., USA) sealed with 5 μm thickness polypropylene film (no. 3520 - Spex Ind. Inc., USA) and dried at 60°C in a laboratory oven. This procedure was carried out twice. The samples were analyzed in triplicate using a rhodium (Rh) X-ray tube at 50 kV and auto-tunable current with a deadtime at 30% and a 3-mm collimator. The X-ray spectrum of the sample was acquired utilizing a Si (Li) detector for 200 s. The quantification was performed using external standard calibration. The recovery of this method was assessed spiking the sample with 1,000 mg Cu L^{-1} before the dry ashing digestion step.

µ-XRF chemical images

The microanalysis was carried out using a benchtop micro-X-ray fluorescence spectroscopy (µ-XRF) system (Orbis PC EDAX, USA) operating with a Rh X-ray tube at 40 kV and 300 µA. The sample was interrogated with a 30 µm X-ray beam spot size provided by a polycapillary optic. The detection was carried out by a 30 mm^2 silicon drift detector (140 eV FWHM at the 5.9 keV Mn-Kα line) with a deadtime of nearly 3%. Seed maps were registered using a matrix of 64x50 points (number of analyzed points on xy-axes) and dwell time per pixel of 1 s. For the primary roots, a matrix of 32x25 points and 500 µs of dwell time were selected. The experimental setup is illustrated in Figure S1.

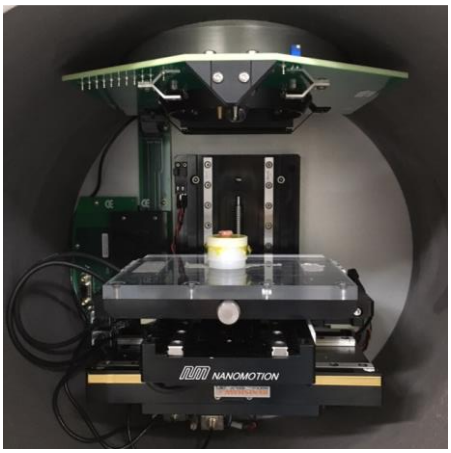

Figure S1. µ-XRF experimental setup, at the LIN-CENA-USP, Piracicaba, Brazil. We used this tool to map the Cu distribution in the bean seeds.

µ-XANES analysis

The experimental setup of the µ-XANES analysis at the XRF beamline in LNLS is illustrated in Figure S2.

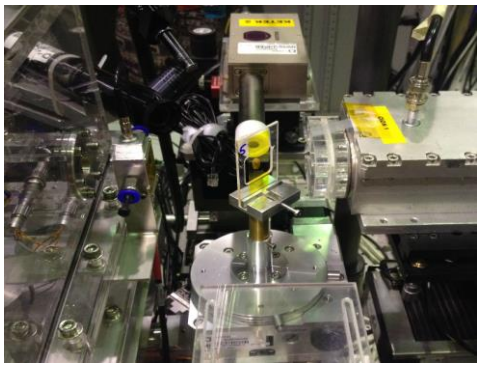

Figure S2. µ-XANES experimental setup at XRF beamline of the LNLS, Campinas, Brazil. One can observe the split bean seed assembled on a Kapton™ tape.

Surface reactivity of CuO nanoparticles

Figure S3. Experimental setup for the nCuO reactivity analysis. The tested material, water and H_2O_2 were loaded in the reaction flask. The production of O_2 via H_2O_2 was monitored measuring the volume of water shifted in the column.

<u>Contents from the results section of the main manuscript</u>

nCuO characterization

The results of purity and contaminant analysis of each bulk nCuO are described in Table S2 and the XRF spectra in the Figure S4.

Table S2. Degree of purity of each nCuO used in this study and concentrations of contaminants found.

CuO size (nm)	**Purity (%)**	**Contaminants (mg kg^{-1})**		
		Cr	**Ca**	**Sn**
25	100%	---	---	---
40	>99.9%	418	---	---
<80	>99.6%	---	1764	2095

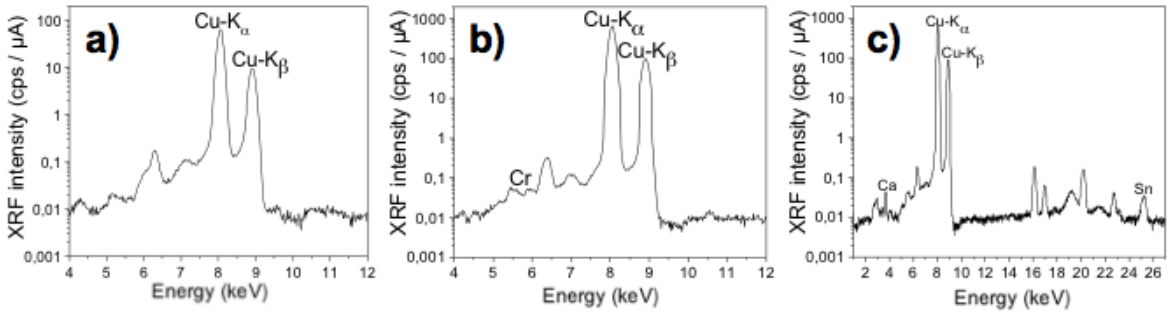

Figure S4. XRF spectra of the differently sized nCuO materials used in this study. a) 25 nm; b) 40 nm and c) <80 nm. The peaks highlight the presence other metals besides Cu, for example Ca, Cr and Sn.

Figure S5 shows the diffractograms of each nCuO provided by the XRD analysis. Scherrer analysis presumed a spherical crystallite shape for both 40 and 80 nm nCuO (Table S3), once similar sizes were found for different planes. These results were in good agreement with the observations by scanning electron microscopy (SEM) (Figure S6).

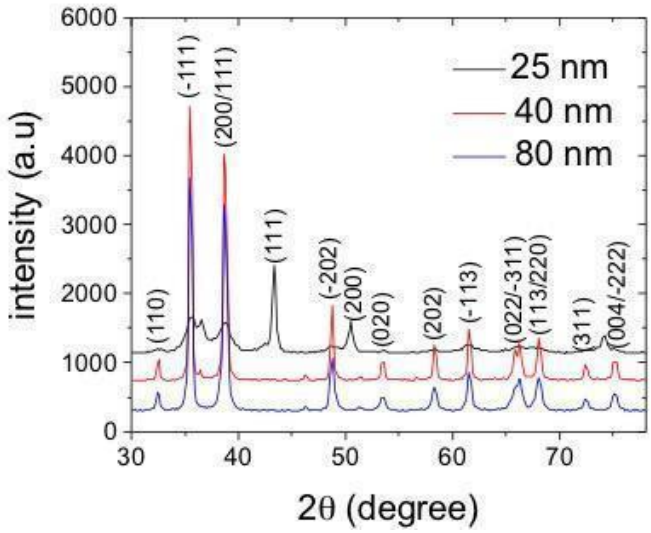

Figure S5. XRD patterns for 25, 40 and <80 nm nCuO. The data shows that the 25 and 40 nm particles are CuO, whereas the 25 nm particles contain a mixture of CuO and metallic Cu.

Table S3. Crystallite size (D) of nCuO (25, 40 and 80 nm) in different planes.

	$D_{(hkl)}$ (nm)		
Plane (oxidic)	**CuO 25 nm**	**CuO 40 nm**	**CuO 80 nm**
-111	---	41.40	32.2
111	3.91	23.00	21.00
-202	---	23.75	17.05

Plane (metallic)	CuO 25 nm	CuO 40 nm	CuO 80 nm
111	5.21	---	---
200	6.47	---	---

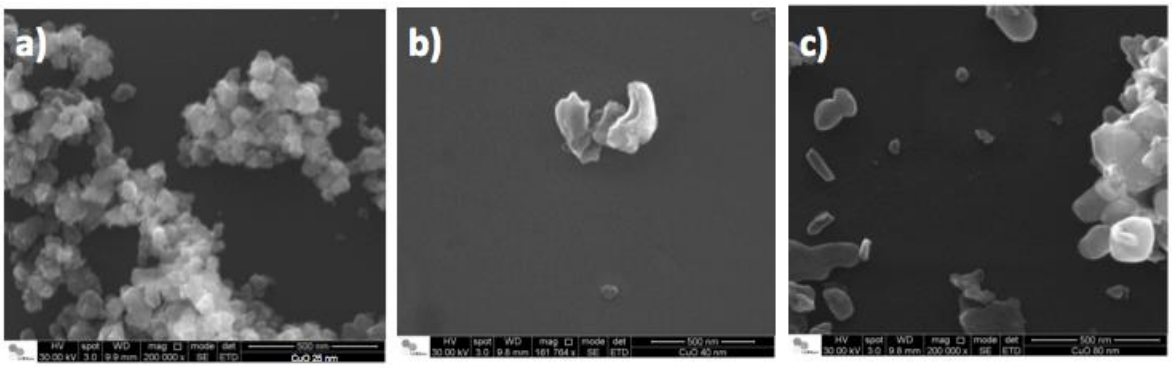

Figure S6. Size and morphology of bulk nCuO observed by scanning electron microscopy (SEM; scale bar: 500 nm). (a) CuO 25 nm; (b) CuO 40 nm and (c) CuO <80 nm.

Dispersions of nCuO at 100 mg L^{-1} were used to determine the hydrodynamic diameter and 10 mg L^{-1} for measuring the surface potential (Table S4).

Table S4. Zeta potential and hydrodynamic diameter of the nCuO (25, 40 and 80 nm) dispersions determined by Dynamic Light Scattering (DLS).

Nominal size	Zeta-potential	Hydrodynamic Diameter (nm)	
(nm)	**(mV)**	*Peak 1*	*Peak 2*
25	-21 ± 5	428 (98.1%)	5477 (1.9%)
40	-15 ± 6	180 (100%)	-------
<80	-25 ± 7	273 (100%)	-------

The linear combination fit for Cu-K edge XAS spectra recorded for the 25 nm CuO-based nanomaterial is presented in Figure S7.

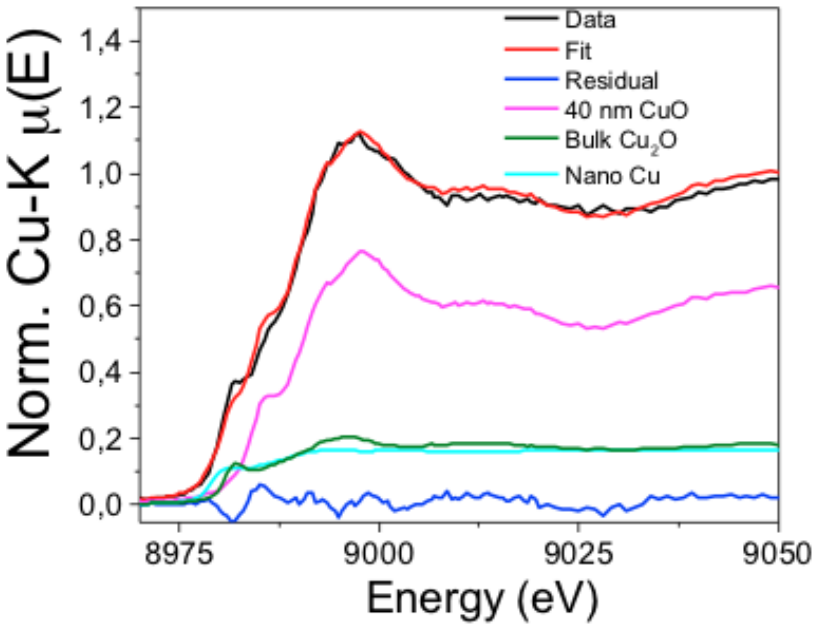

Figure S7. Linear combination fit for Cu-K edge XAS spectra recorded for the 25 nm CuO based nanomaterial. The 25 nm CuO nanoparticle was a mixture of CuO (65 ± 2 %), Cu_2O (18 ± 4%) and Cu (17 ± 10%).

Statistical analysis

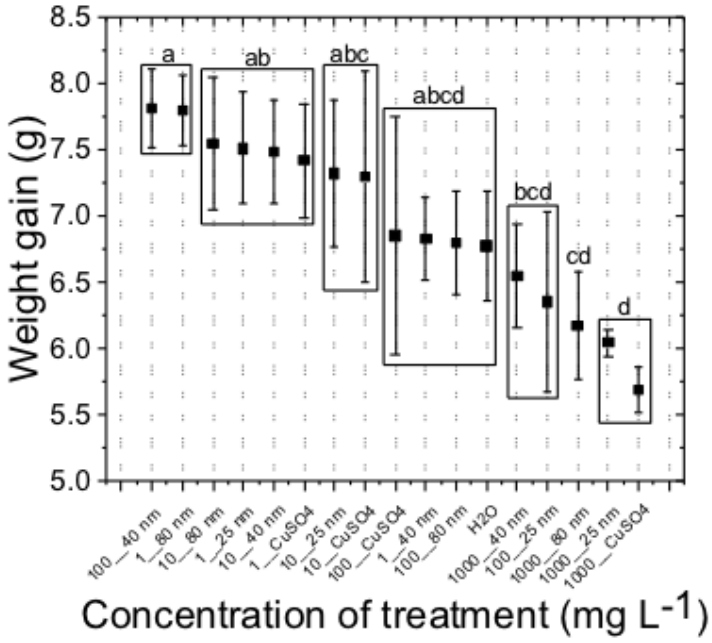

Figure S8. Weight gain of bean (*Phaseolus vulgaris*) seeds as function of the concentration of nCuO and $CuSO_4$ (in mg Cu L^{-1}). The data points followed by the same letter were significantly different according to the Tukey test at $p<0.05$.

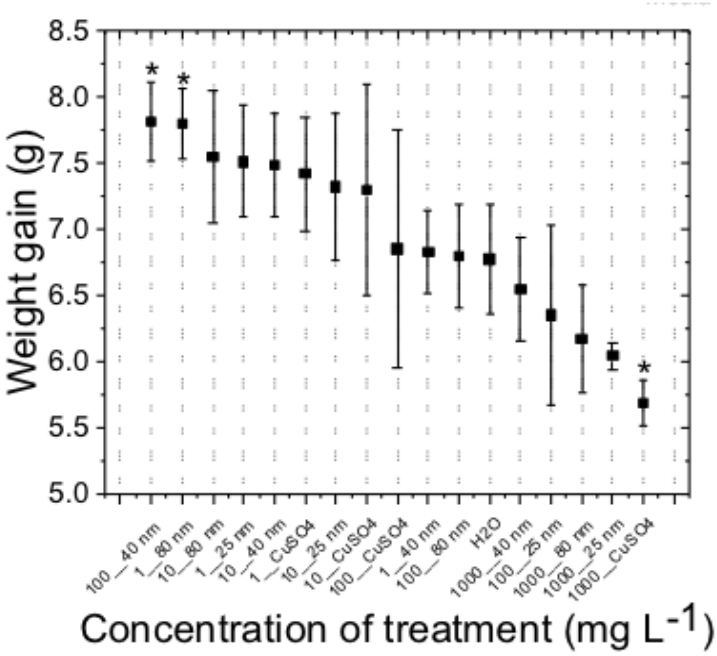

Figure S9. Weight gain of bean (*Phaseolus vulgaris*) seeds as function of the concentration of nCuO and $CuSO_4$ (in mg Cu L^{-1}). According to the Dunnett's test at $p<0.05$ the treatments marked with asterisk are significantly different from the negative control: 100 mg Cu L^{-1} 40 nm nCuO, 1 mg Cu L^{-1} 80 nm nCuO and 1,000 mg Cu L^{-1} $CuSO_4$.

Copper determination

The Cu content of the seedlings was determined by EDXRF. The two fractions of the seedlings (seedling and seed coat) were analyzed individually (Figure S10).

Figure S10. Seed coat and seedling of a common bean (*Phaseolus vulgaris*). These parts were separated to determine the Cu content shown in Figure 3 of the main manuscript.

nCuO solubility

To verify the Cu solubility of each nCuO powder size, 50 mL of nCuO aqueous dispersions were prepared at 100 and 1,000 mg Cu L^{-1} using a probe ultrasonic device (Fisher Scientific™ Model 705 Sonic Dismembrator). The equipment was operated at 95 W (amplitude of 50 %) and 50 J, during 4 x 5 min with an interval of 3 min between each cycle. After 24 hours, one milliliter of each dispersion was transferred to Eppendorf tubes and then centrifuged by a microcentrifuge (Mikro 120, Hettich, Germany) for 60 minutes at 13,000 rpm.

Quantitative analysis of the supernatants was performed by EDXRF (EDX-720, Shimadzu, Japan) using the thin film method. Fifteen milliliters of the supernatants were dripped in a 6.3 window cuvette (no. 3577 - Spex Ind. Inc., USA) assembled with a five micrometer thick polypropylene film, and dried at 60°C in a laboratory oven. After repeating this procedure twice, the samples were measured in triplicate using a rhodium (Rh) X-ray tube operating at 50 kV, auto-tunable current with a deadtime below 30% and using a 3-mm collimator. A Si(Li) detector acquired the X-ray spectra during 200 s. The quantification was performed using external standard calibration and Ga as internal standard. The measurements were performed in triplicate. The quantitative results are presented in the Figure S11.

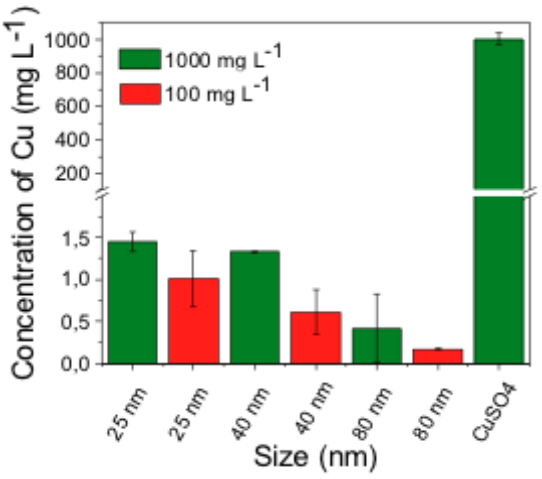

Figure S11. Cu soluble fraction in the supernatant of nCuO (25, 40 and 80 nm) dispersions. The concentration of soluble Cu was higher for the 1,000 mg Cu L^{-1} than for 100 mg Cu L^{-1} dispersions.

μ-XRF chemical images

The acquired chemical images for Cu and K of the treated seeds are presented from Figures S12-S14.

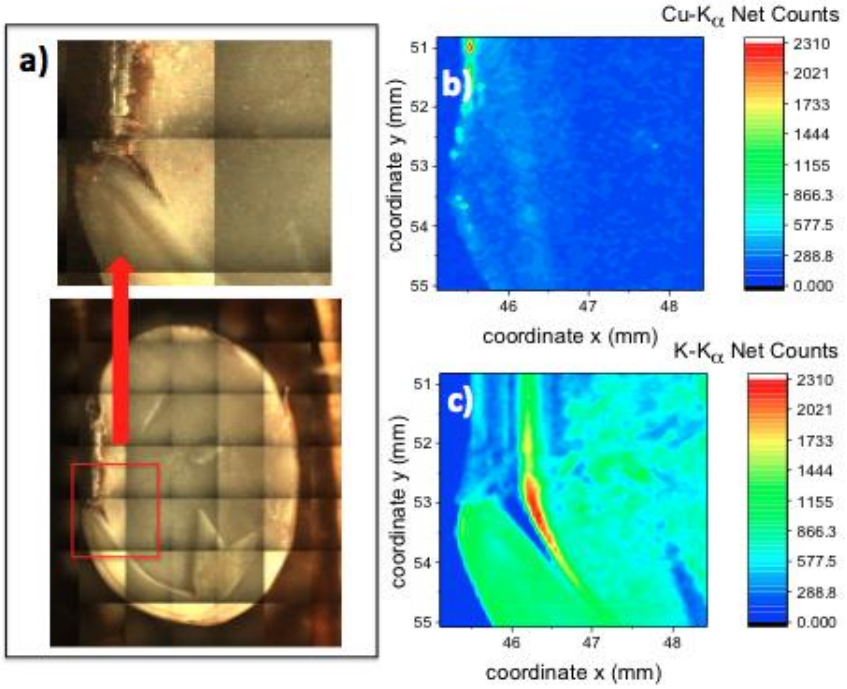

Figure S12. (a) Picture of a common bean (*Phaseolus vulgaris*) highlighting its selected mapped area; and corresponding 2D chemical location of (b) Cu and (c) K in a seed treated with nCuO 80 nm at 1,000 mg Cu L^{-1}. Cu was mainly concentrated in the seed coat.

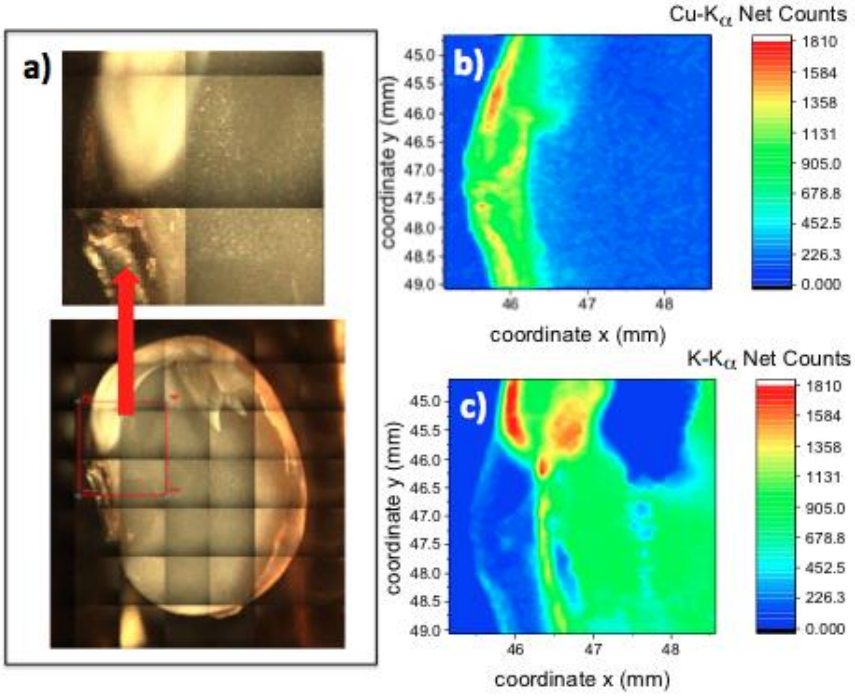

Figure S13. (a) Picture of a common bean (*Phaseolus vulgaris*) highlighting its selected mapped area; and its corresponding 2D chemical location of (b) Cu and (c) K in a seed treated with nCuO 25 nm at 1,000 mg Cu L^{-1}. Copper was mainly found in the seed coat.

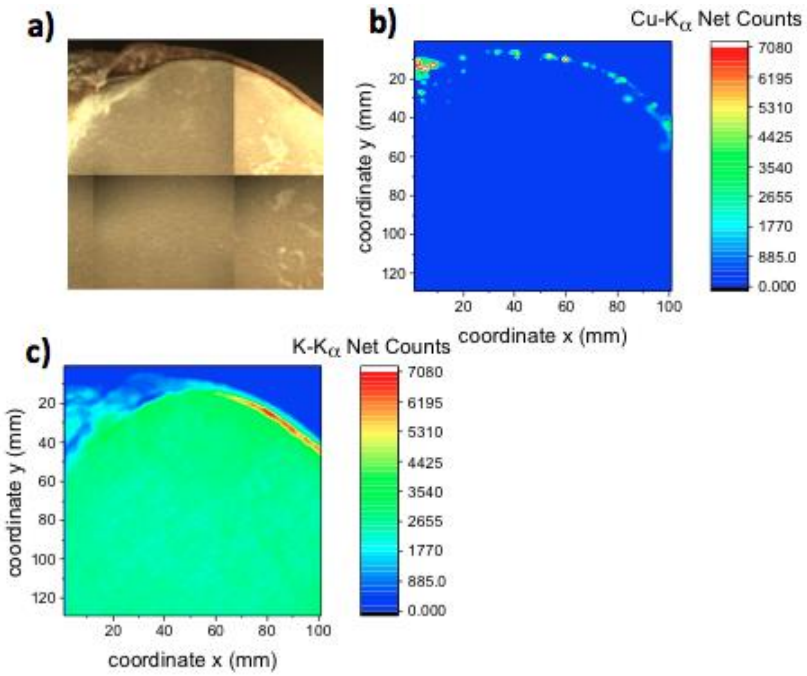

Figure S14. (a) Picture of a common bean (*Phaseolus vulgaris*) highlighting its selected mapped area; and corresponding 2D chemical location of (b) Cu and (c) K in a seed treated with nCuO 40 nm at 5,000 mg Cu L^{-1}. Cu hotspots were found in the seed coat.

μ-XANES analysis

Figures S15-S17 highlight the specific regions of the seed measured. The linear combination fit for Cu-K edge XAS spectra recorded in the embryo of a seed treated with 40 nm nCuO at 1,000 mg Cu L^{-1} is shown in Figure S18.

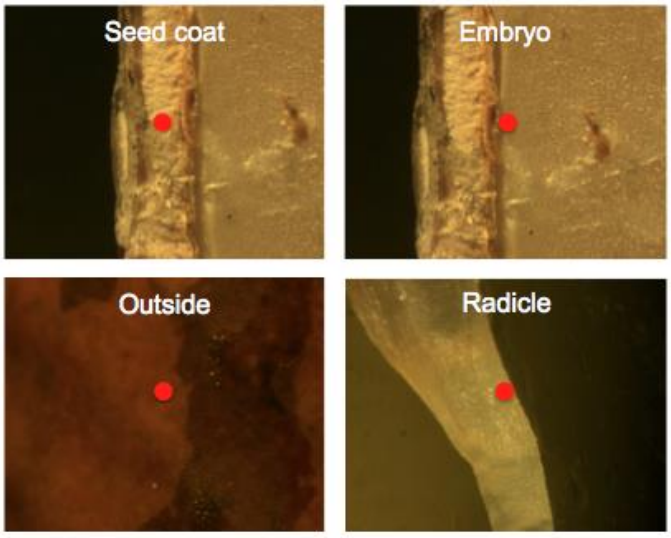

Figure S15. This figure shows the locations in which the μ-XANES spectra were recorded for the bean (*Phaseolus vulgaris*) seeds and radicle primed with 25 nm nCuO. The locations are highlighted by the red spots.

Figure S16. This figure shows the locations in which the µ-XANES spectra were recorded for the bean (*Phaseolus vulgaris*) seeds primed with 40 nm nCuO. The locations are highlighted by the red spots.

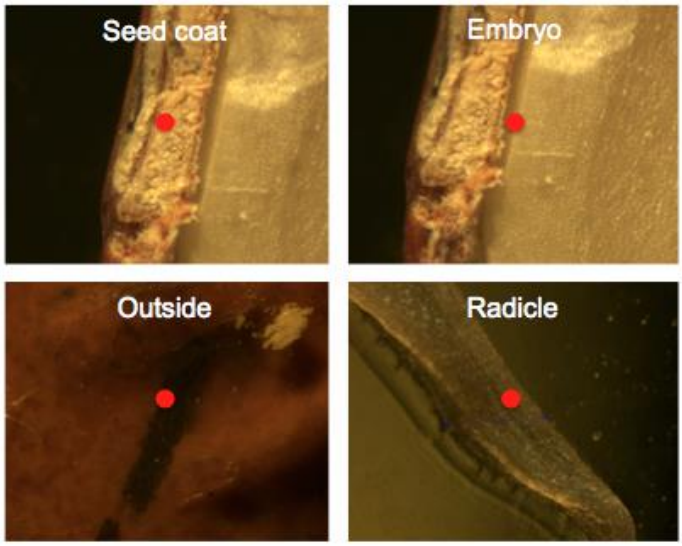

Figure S17. This figure shows the locations in which the µ-XANES spectra were recorded for the bean (*Phaseolus vulgaris)* seeds and radicle primed with 80 nm nCuO. The locations are highlighted by the red spots.

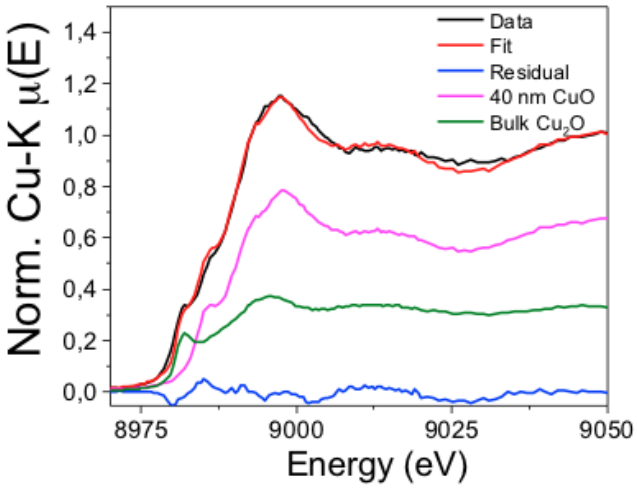

Figure S18. Linear combination fit for Cu-K edge XAS spectra recorded in the embryo of a bean (*Phaseolus vulgaris*) seed treated with 40 nm nCuO at 1,000 mg Cu L^{-1}. The experimental curve, shown in black, could be adjusted as a mixture of 40 nm nCuO (66 ± 1 %) and bulk Cu_2O (34 ± 1 %).

SEM image of the hilum

Phaseolus vulgaris seeds have a hilum associated to the seed coat, this spongy tissue is a scar left by the funiculus, the structure that connects the seed to the placenta[10]. In order to verify the pore size of this tissue, a SEM image was recorded (TM-1000, Hitachi, Tokyo, Japan).

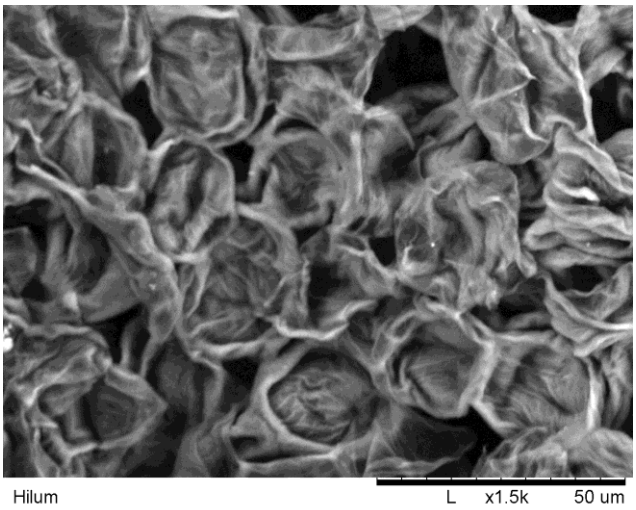

Figure S19. SEM image of the hilum of a common bean (*Phaseolus vulgaris*) seed. The pore size indicates that nanoparticles can enter through this way (scale bar: 50 μm).

Surface reactivity of nCuO

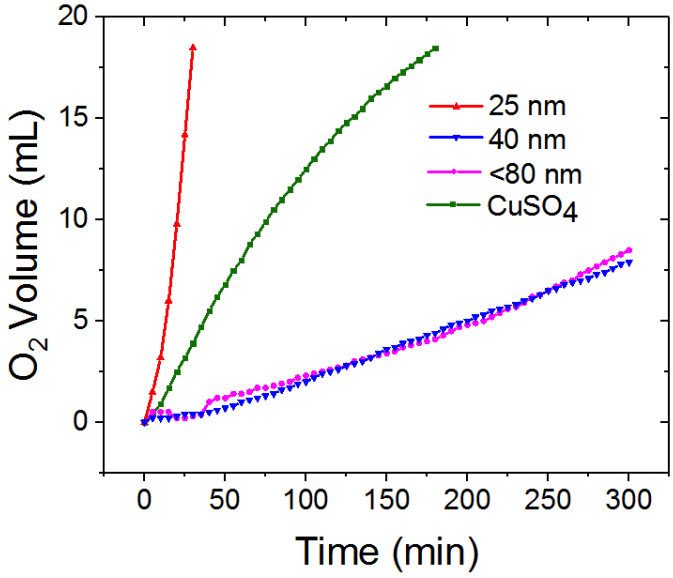

Figure S20. H_2O_2 degradation rate in the presence of $CuSO_4$ and 25, 40 and 80 nm nCuO. The 40 and 80 nm nCuO decomposed the H_2O_2, however they were much slower compared to Cu^{2+} from the sulfate and the 25 nm nCuO. We believe that the core-shell structure played a decisive role increasing the surface reactivity.

References

1. Parveen, A.; Rao, S. Effect of nanosilver on seed germination and seedling growth in *Pennisetum glaucum*. *J. Clust. Sci*. **2015**, 26, 693–701.

2. Thuesombat, P; Hannongbua, S.; Akasit, S.; Chadchawan, S. Effect of silver nanoparticles on rice (*Oryza sativa* L. cv. KDML 105) seed germination and seedling growth. *Ecotox. Environ. Safe*. **2014**, 104, 302-309.

3. Zhang, R.; Zhang, H.; Tu, C.; Hu, X.; Li, L.; Luo, Y.; Christie, P. Phytotoxicity of ZnO nanoparticles and the released Zn(II) ion to corn (*Zea mays* L.) and cucumber (*Cucumis sativus* L.) during germination. *Environ. Sci. Pollut. R*. **2015**, 22, 11109-11117.

4. Gokak, I. B.; Taranath, T. C. Morphological and biochemical responses of *Abelmoschus esculantus* (L.) Moench to zinc nanoparticles. *Adv. Nat. Sci-Nanosci*. **2015**, 6, 25017, 5pp.

5. Nair, P. M. G.; Chung, I. M. The responses of germinating seedlings of green peas to copper oxide nanoparticles. *Biol. Plantarum* **2015**, 59, 591-595.

6. Li, X.; Yang, Y.; Gao, B.; Zhang, M. Stimulation of peanut seedling development and growth by zero-valent iron nanoparticles at low concentrations. *Plos One* **2015**, 10, e0122884.

7. Xiang, L.; Zhao, H. M.; Li, Y. W.; Huang, X. P.; Wu, X. L.; Zhai, T.; Yuan, Y.; Cai, Q. Y.; Mo C. H. Effects of the size and morphology of zinc oxide nanoparticles on the germination of Chinese cabbage seeds. *Environ. Sci. Pollut. R*. **2015**, 22, 10452-10462.

8. Nair, P. M. G.; Chung, I. M. Physiological and molecular level studies on the toxicity of silver nanoparticles in germinating seedlings of mung bean (*Vigna radiata* L.). *Acta Physiol. Plant*. **2015**, 37, 1719.

9. Vannini, C.; Domingo, G.; Onelli, E.; de Mattia, F.; Bruni, I.; Marsoni, M.; Bracale M. Phytotoxic and genotoxic effects of silver nanoparticles exposure on germinating wheat seedlings. *J. Plant. Physiol*. **2014**, 13, 1142–1148.

10. Vieira, C.; Paula Júnior, T. J.; Borém, A. Botânica. In *Feijão*. 2 ed.; Universidade Federal de Viçosa: Viçosa, Brazil, 2006; 600 pp.